Journal of Alloys and Compounds 915 (2022) 165453

Contents lists available at ScienceDirect

Journal of Alloys and Compounds

journal homepage: www.elsevier.com/locate/jalcom

Research Article

Enhanced photoluminescence of GeSn by strain relaxation and spontaneous carrier confinement through rapid thermal annealing

Guangyang Lin[a], Kun Qian[a], Hongjie Cai[a], Haochen Zhao[b], Jianfang Xu[a], Songyan Chen[a], Cheng Li[a,*], Ryan Hickey[b], James Kolodzey[b], Yuping Zeng[b,*]

[a] Department of Physics, Xiamen University, Xiamen, Fujian 361005, People's Republic of China
[b] Department of Electrical and Computer Engineering, University of Delaware, Newark, DE 19716, United States

ARTICLE INFO

Article history:
Received 8 February 2022
Received in revised form 12 May 2022
Accepted 13 May 2022
Available online 17 May 2022

Keywords:
Germanium tin
Rapid thermal annealing
Photoluminescence
Strain relaxation
Gradual heterojunction

ABSTRACT

In this work, the structural evolution and photoluminescence (PL) of 200 nm pseudomorphic $Ge_{0.9338}Sn_{0.0662}$ on Ge (001) substrate grown by low-temperature molecular beam epitaxy (MBE) after rapid thermal annealing (RTA) is studied. Under RTA at 350 °C or lower, the GeSn film is coherently strained on Ge substrate. As RTA temperature further increases, gradual strain relaxation of GeSn is enabled by generation of misfit dislocations and threading dislocations. As RTA temperature reaches 550 °C or beyond, Sn segregation occurs along with strain relaxation. The PL intensity of annealed samples is enhanced compared to that of as-grown sample probably due to improved crystal quality and strain relaxation (for RTA at > 350 °C) of GeSn. The sample annealed at 500 °C exhibits highest PL intensity due to formation of a Sn-component-graded (SCG) heterojunction with highest Sn content in surface region resulted from interdiffusion of Ge and Sn. The formation of SCG heterojunction renders spontaneous confinement of optically pumped carriers in the surface region and enlarges occupation probability of carriers in Γ valley. Additionally, the carrier confinement in the surface region reduces self-absorption of GeSn and suppresses nonradiative recombination near the GeSn/Ge interface. The results manifest that RTA is an appropriate approach to improve the light emitting property of GeSn grown by low-temperature MBE.

1. Introduction

Germanium tin (GeSn) has attracted abundant researches in recent years due to its preeminent optoelectronic properties and compatibility with silicon (Si) based complementary metal-oxide-semiconductor (CMOS) process. Through incorporation of Sn into Ge, the bandgap of GeSn can be tuned from near-infrared (NIR) to mid-infrared (MIR) range [1,2]. Moreover, as Sn content increases, GeSn could transform to a direct bandgap material rendering GeSn a promising material for Si photonics, especially for the light source module, which is the bottleneck for Si photonics. The cross point of indirect and direct bandgap transition of GeSn without strain is predicted to occur at a Sn content of ~ 8% [3–7], To date, GeSn-based light emitting diodes [8–11], optically pumped lasers [3,12–15] and even electrically pumped lasers [16,17] working at NIR and MIR ranges have been realized. However, current GeSn-based light emitting devices suffer from high injection conditions and/or low working temperatures due to lack of high-quality direct bandgap GeSn material.

The growth of high-quality direct bandgap GeSn material faces two main challenges: low solid solubility of α-Sn in Ge (< 1%) [18] and large lattice mismatch between Sn and Ge [19]. The former hinders acquisition of Sn-rich GeSn alloys and limits the maximum post-processing temperature of GeSn. The latter induces compressive strain in GeSn resulting in higher Sn content to transform GeSn into direct bandgap material [20]. Several nonequilibrium growth methods have been proposed to obtain Sn-rich GeSn alloys, such as molecular beam epitaxy (MBE) [21–24], chemical vapor deposition (CVD) [25–28] and magnetron sputtering [29,30]. However, to avoid Sn segregation from the film [31], the growth temperature has to be set at low values, especially for MBE, which has much lower growing rates than those of CVD. The typical growth temperature of GeSn by MBE is less than 200 °C [21,32]. The low-temperature growth during MBE leads to high-density point defects in GeSn film thus degrades the performance of GeSn-based optoelectronic devices [33,34]. Additionally, low-temperature MBE growth impedes the relaxation of the compressive strain in GeSn due to insufficient kinetics of Ge and Sn atoms at low temperature [35,36]. Alternative approaches are

* Corresponding authors.
E-mail addresses: lich@xmu.edu.cn (C. Li), yzeng@udel.edu (Y. Zeng).

https://doi.org/10.1016/j.jallcom.2022.165453
0925-8388/

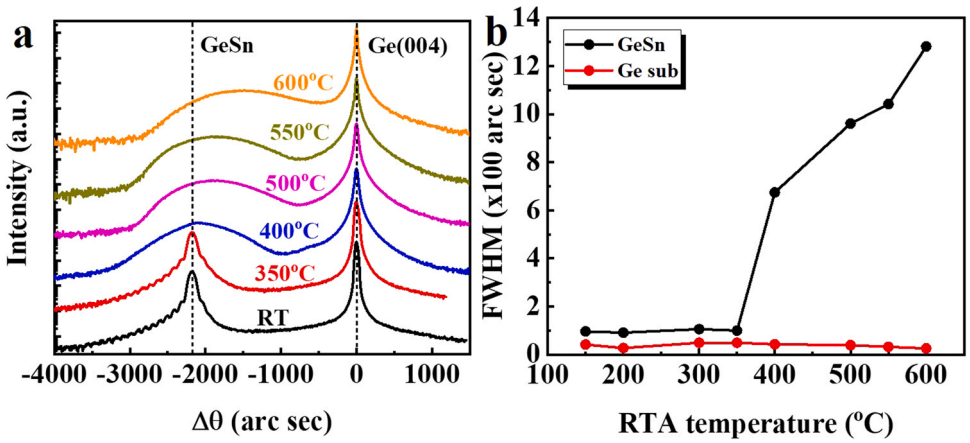

Fig. 1. (a) Symmetric (004) XRD ω-2θ rocking-curve scans showing diffraction intensity versus diffraction angle of GeSn grown on Ge substrate by MBE before (black curve) and after (red to yellow curves) RTA at 350–600 °C; The peak position of Ge substrate in each plot has been shifted to zero for better comparison. (b) Dependence of FWHM for Ge (red curve) and GeSn (black curve) (004) XRD peaks on RTA temperature.

required to improve the material quality and/or relax the compressive strain of GeSn grown by low-temperature MBE.

Post thermal annealing is a valid approach to improve the crystal quality and/or relax the lattice strain of epilayers. The influence of thermal annealing on strain relaxation and Sn segregation of GeSn has been studied by many groups [37–39]. However, the results are far from being conclusive. Some researchers indicate that the compressive strain in GeSn films can be relaxed by thermal treatment [37], while some investigations show that Sn segregates without strain relaxation in the GeSn film under thermal treatment [40,41]. The influence of thermal treatment on the structure of GeSn needs to be further explored. In addition, few studies report on the influence of thermal treatment on the optoelectronic properties of GeSn [42,43], especially the light emitting property of GeSn grown by low-temperature MBE.

In this work, the influence of rapid thermal annealing (RTA) on the structural and optical properties of 200 nm fully strained $Ge_{0.9338}Sn_{0.0662}$ on Ge substrate grown by low-temperature MBE is studied. As RTA temperature rises, strain relaxation is observed prior to Sn segregation in the GeSn film. Interdiffusion of Ge and Sn is detected under RTA at high temperature. The photoluminescence (PL) intensity of annealed samples is enhanced compared to that of as-grown samples. The PL intensity of the sample annealed at 500 °C is enhanced by more than 7.8 fold compared to that of an as-grown sample. The results show that RTA is an effective approach to improve the light emitting efficiency of GeSn grown at low temperature.

2. Experimental section

The GeSn sample was grown on a 3-inch undoped (001) oriented Ge substrate with a resistivity of 40 Ω cm by molecular beam epitaxy (MBE). The Ge substrate was chemically cleaned based on the procedure developed by Hovis et al. [44] then was immediately loaded into the MBE preparation chamber after formation of a Ge oxide protective layer. After an overnight degassing process, the substrate was transferred to the growth chamber with a base pressure of 3×10^{-10} Torr. Prior to GeSn deposition, the substrate was flashed to 850 °C for 10 min to desorb the Ge oxide. Next, the substrate heater was ramped down to 150 °C for GeSn growth. The Ge and Sn fluxes were provided by thermal evaporation of triple zone-refined Ge and Sn (6 N, United Mineral and Chemical Corporation) loaded in Knudsen thermal effusion cells, respectively. The Ge and Sn cell temperatures were kept at 1220 °C and 980 °C during growth, respectively. After a growth period of 3 h, a GeSn film with thickness of ~ 195 nm and Sn content of ~ 6.6% was expected to be deposited on Ge substrate, based on deposition rates for Sn and Ge. The sample was then cleaved into pieces of 1 cm^2 for post-processing studies. Rapid thermal annealing (RTA) was carried out at 200–600 °C for 1 min in N_2 during different batches.

X-ray diffraction (XRD, Panalytical X′ Pert) rocking curves and reciprocal space mapping (RSM), Raman spectra (ThermoScientific DXR Raman microscope), transmission electron microscope (TEM, FEI Talos F200X) images and X-ray energy dispersive spectra (EDS, Oxford) were taken to characterize Sn distribution, strain evolution and crystal quality of GeSn after thermal treatments. The surface morphology of GeSn after RTA was scanned by atomic force microscope (AFM, Anasys NanolR_2) using tapping mode. Photoluminescence spectra were collected by a home-made PL measurement system to analyze the optoelectronic property of GeSn after RTA.

3. Results and discussion

Fig. 1(a) compares the (004) XRD ω-2θ rocking-curve scans of the as-grown sample and samples after RTA at 350–600 °C. The peak position of Ge substrate in each plot has been shifted to zero for better comparison. The peaks located between − 500 to − 2100″ are from GeSn. For the as-grown sample (black curve), Pendellösung fringes are observed indicating that the GeSn film is coherently strained with respect to the Ge substrate. From the peak separation between Ge and GeSn and the periodicity of the fringes, the Sn content and thickness of the GeSn film are extracted to be 6.62% and 200 nm, respectively. After RTA at temperatures up to 350 °C (red curve, curves for GeSn annealed at temperatures below 350 °C are not shown), the GeSn peak position barely changes and the Pendellösung fringes are clear suggesting that the GeSn film is still fully strained. As annealing temperature elevates to 400 °C (blue curve), the Pendellösung fringes disappear and the GeSn peak broadens accompanied by a slight shift of peak position to higher angle side. The disappearing of fringes indicates that the interface between GeSn and Ge becomes blurry, which may be due to strain relaxation and generation of misfit dislocations. For samples annealed at 500–600 °C (purple curve to yellow curve), the GeSn peaks are asymmetric. As temperature increases, the GeSn peak becomes broader and shifts closer to the Ge peak. Fig. 1(b) summarizes the dependence of the full width at half maximum (FWHM) of GeSn and Ge (004) XRD peaks on RTA temperature. For Ge peak, as RTA temperature increases, the FWHM varies between 26″ and 49″. For GeSn peak, the FWHM remains at a small value of ~ 100″ at RTA temperatures of 350 °C or lower. As RTA temperature rises to 400, 500,

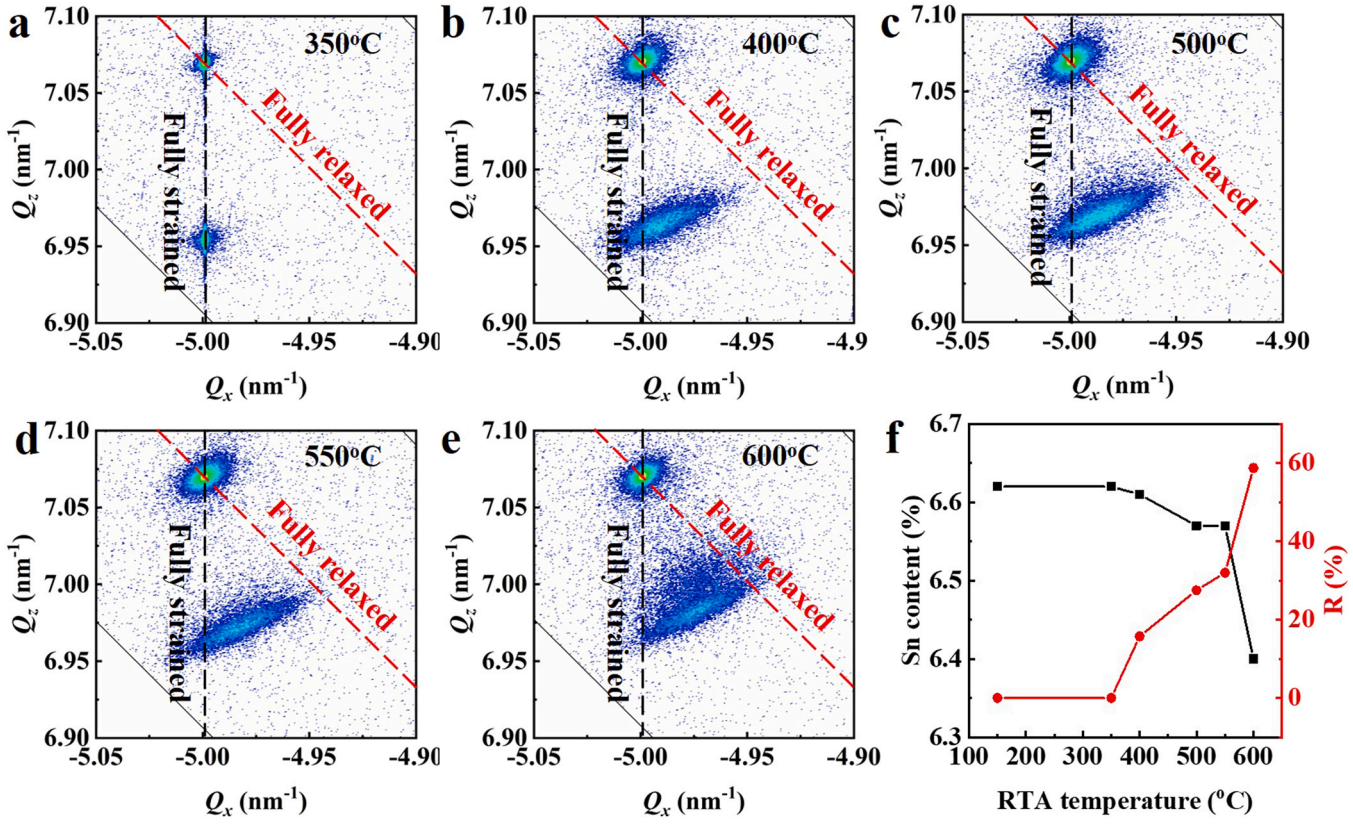

Fig. 2. Asymmetric ($\bar{2}\bar{2}4$) XRD-RSMs of GeSn on Ge sample after RTA at (a) 350 °C, (b) 400 °C, (c) 500 °C, (d) 550 °C and (e) 600 °C. GeSn peaks centered on the black and red dashed lines indicate that the GeSn films are fully strained and fully relaxed to Ge substrate, respectively. (f) Dependence of Sn content (black curve) and degree of strain relaxation (red curve) of the GeSn films extracted from XRD-RSMs on RTA temperature.

550 and 600, the FWHM of GeSn (004) XRD peak dramatically increases to 674, 961, 1041 and 1281″, respectively. The surge of FWHM for GeSn peak along ω-2θ direction is attributed to variation in lattice plane spacing (*d* spacing) with depth and may result from Sn diffusion and/or generation of dislocations along the growth direction of the GeSn film after thermal treatment.

To quantitatively characterize the evolution of Sn content and strain in the GeSn films after RTA, asymmetric ($\bar{2}\bar{2}4$) XRD-RSMs of samples after RTA at 350–600 °C are taken, as shown in Fig. 2. The maps were collected as area scans using ω-2θ scans offset along the ω axis. In the RSM, the intensity of the diffracted beam is depicted as contour lines of equal intensity as a function of the reciprocal lattice vectors along the [$\bar{1}\bar{1}$0] ($Q_{//}$) and [001] ($Q_{\perp}$) directions. The upper contour peak and lower contour peak in each map are from the diffraction of Ge substrate and GeSn film, respectively. The vertical dash line (black) in each map indicates the line of full strain, since a layer peak centered on this line would have an identical in-plane lattice constant to Ge substrate, the oblique dash line (red) in each map represents the line of complete strain relaxation, since peaks centered on this line have equal in-plane and out-of-plane lattice constants. For the sample annealed at 350 °C (Fig. 2(a)), Ge and GeSn peaks have an identical $Q_{//}$ confirming that the GeSn film is fully strained on Ge substrate. After RTA at 400 °C (Fig. 2(b)), both the Ge and GeSn peaks broaden along ω direction (the direction of ω and ω-2θ scans have been indicated in Fig. 2(b)), which is presumably due to formation of dislocations. As RTA temperatures further rises, the GeSn peak gradually shifts toward the fully relaxed line implying larger strain relaxation of the GeSn film. Additionally, for the sample annealed at 600 °C, the GeSn peak shows a tail along ω-2θ direction toward the Ge peak suggesting formation of lower Sn-content GeSn, which indicates Sn loss from the film. From the separation in $Q_{//}$ and $Q_{\perp}$ between Ge and GeSn peaks, the lattice constant of the GeSn parallel ($a_{//GeSn}$) and perpendicular($a_{\perp GeSn}$) to the substrate plane can be calculated by [45]:

$$a_{//GeSn} = \frac{Q_{//Ge} - Q_{//GeSn}}{Q_{//GeSn}} a_{Ge} + a_{Ge}, \tag{1}$$

$$a_{\perp GeSn} = \frac{Q_{\perp Ge} - Q_{\perp GeSn}}{Q_{\perp GeSn}} a_{Ge} + a_{Ge}, \tag{2}$$

where a_{Ge} = 0.5658 nm is the lattice constant of the Ge substrate. The peak position ($Q_{//}$, $Q_{\perp}$) at which maximum diffraction intensity locates is used for calculation. The bulk lattice constant of GeSn (a_{0GeSn}) can be then obtained by:

$$a_{0GeSn} = a_{\perp GeSn} + \frac{2\upsilon_{GeSn}(a_{//GeSn} - a_{\perp GeSn})}{1 + \upsilon_{GeSn}}, \tag{3}$$

where υ_{GeSn} = 0.262[21] is the respective [100] Poisson's ratio of GeSn and is estimated by interpolating the values of Ge (υ_{Ge} = 0.26) and α-Sn (υ_{Sn} = 0.29). The Sn content (x) of the GeSn film could consequently be deduced by:

$$x = \frac{a_{0GeSn} - a_{Ge}}{a_{Sn} - a_{Ge}}, \tag{4}$$

where a_{Sn} = 0.6489 nm is the lattice constant of α-Sn. Based on Eqs. (1)–(3), the in-plain strain ($\varepsilon_{//}$) and out-of-plane strain ($\varepsilon_{\perp}$) of GeSn could be calculated by:

$$\varepsilon_{//} = \frac{a_{//GeSn} - a_{0GeSn}}{a_{0GeSn}}, \tag{5}$$

$$\varepsilon_{\perp} = \frac{a_{\perp GeSn} - a_{0GeSn}}{a_{0GeSn}}. \tag{6}$$

Ultimately, the strain relaxation (R) of GeSn can be acquired by:

Table 1
List of Sn content (x), in-plane strain ($\varepsilon_{//}$), out-of-plane strain ($\varepsilon_{\perp}$) and strain relaxation (R) of GeSn films after RTA at different temperatures extracted from the XRD-RSMs.

T (°C)	x (%)	$\varepsilon_{//}$ (%)	$\varepsilon_{\perp}$ (%)	R (%)
150 (As-grown)	6.62	-0.96	0.68	0
350	6.62	-0.96	0.68	0
400	6.61	-0.81	0.58	15.76
500	6.57	-0.69	0.49	27.52
550	6.57	-0.65	0.46	31.99
600	6.40	-0.38	0.27	58.75

$$R = \frac{a_{//GeSn} - a_{Ge}}{a_{0GeSn} - a_{Ge}}. \quad (7)$$

Table 1 summarizes the Sn content (x), in-plane strain ($\varepsilon_{//}$), out-of-plane strain ($\varepsilon_{\perp}$) and strain relaxation (R) of the GeSn films after RTA at different temperatures extracted from the XRD-RSMs based on Eqs. (1)–(7). The dependence of Sn content (black curve) and strain relaxation (red curve) on RTA temperature is plotted in Fig. 2(f). The GeSn film maintains fully compressive strain with a Sn content of 6.62% after RTA at 350 °C. As annealed at 400 °C, the Sn content slightly decreases to 6.61% and the in-plane strain decreases from −0.96% to −0.81% corresponding to a strain relaxation of 15.76%. After RTA at 500 and 550 °C, the Sn content of the GeSn film drops to 6.57%, the in-plane strain relaxes to −0.69% and −0.65% corresponding to a strain relaxation of 27.52% and 31.99%, respectively. For the sample annealed at 600 °C, the Sn content further reduces to 6.40% indicating Sn segregation from the film. A strain relaxation of 58.75% occurs resulting in an in-plane strain of −0.38% in the GeSn film.

The XRD-RSM results indicate that the strain relaxation of GeSn can be enabled by RTA at 400 °C or higher. However, Sn loss occurs during RTA at high temperature. To study the evolution of GeSn surface morphology after RTA, AFM scans were then conducted. Fig. 3 compares the surface AFM images of the GeSn samples annealed at different temperatures. An area of $5 \times 5\ \mu m^2$ is randomly selected for each sample for measurements. The surface of as-grown sample is very smooth exhibiting a roughness root-mean-square (RMS) of 0.56 nm, as shown in Fig. 3(a). After RTA at 350 °C, the sample maintains a flat surface with a roughness RMS of 0.54 nm, as displayed in Fig. 3(b). For the sample annealed at 400 °C (Fig. 3(c)), cross-hatched pattern appears with a surface roughness RMS of 0.49 nm. The formation of cross-hatched pattern confirms strain relaxation through gliding of dislocations along < 111 > facets [46], agreeing well with the XRD-RSM result. As annealing temperature elevates to 500 °C (Fig. 3(d)), some nano-holes were observed along with the cross-hatched pattern. The surface roughness rises to 1.14 nm. From the XRD-RSM result, it is found that the Sn content of GeSn film slightly decreases from 6.61% to 6.57% after RTA at 500 °C. The formation of nano-holes can be ascribed to Sn desorption consequently. For the sample annealed at 550 °C, the surface is decorated with nano-trenches and clusters due to stronger Sn segregation and migration [38] resulting in a surface roughness RMS of 3.04 nm, as shown in Fig. 3(e). After RTA at 600 °C (Fig. 3(f)), the surface is covered by nano-islands and holes due to severe Sn segregation and migration [38]. The surface roughness RMS dramatically goes up to 9.20 nm.

From AFM scans, it is indicated that Sn is released from the GeSn film and migrates on the surface during RTA at high temperatures. To further investigate the influence of thermal treatment on the surface region of the GeSn samples, Raman spectra were taken using a 532 nm laser as excitation light, which has a penetration depth of < 20 nm in GeSn. Fig. 4(a) shows the Raman spectra of the as-grown sample and samples after RTA at 350–600 °C. The resolution

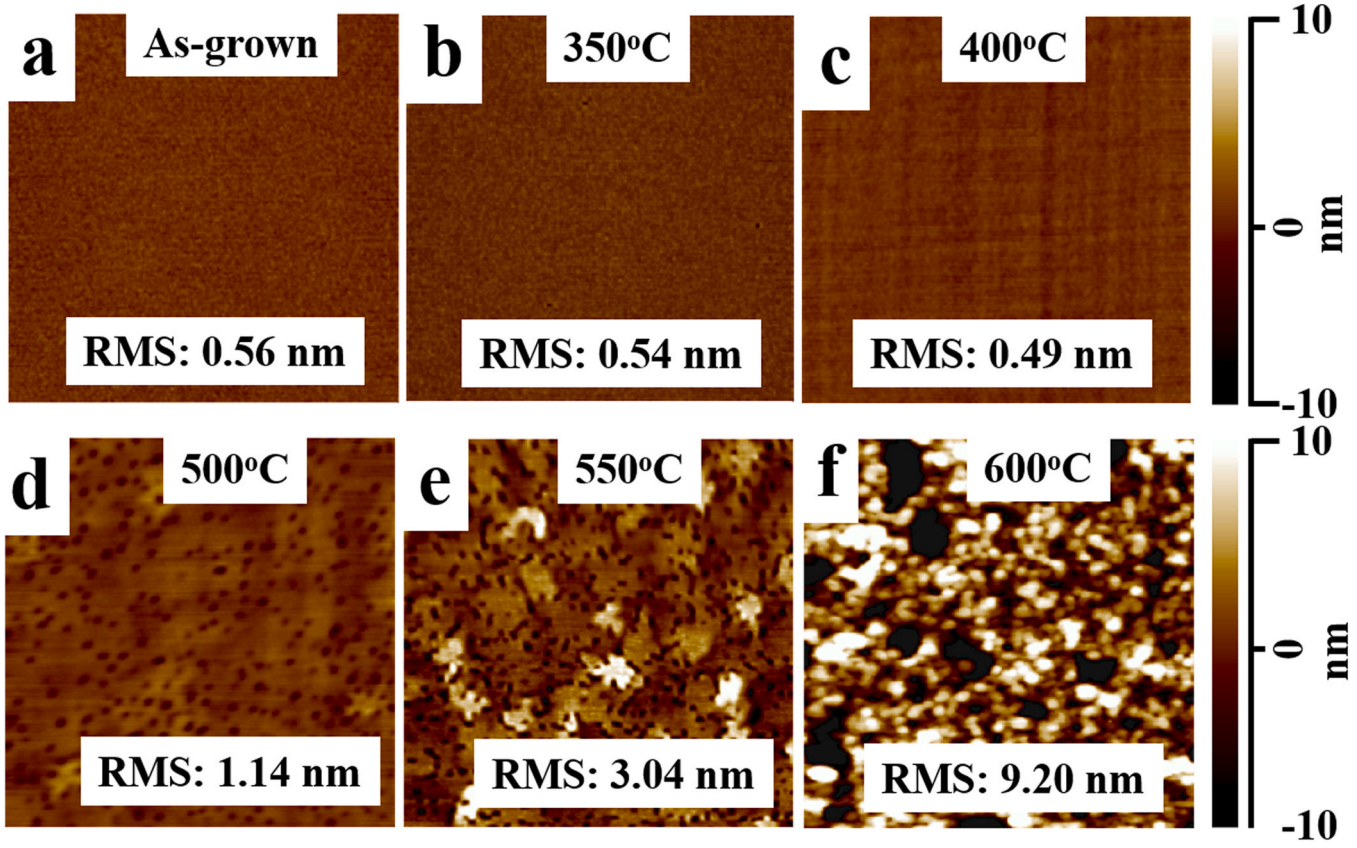

Fig. 3. Surface morphology of (a) as-grown sample and samples after RTA at (b) 350 °C, (c) 400 °C, (d) 500 °C, (e) 550 °C and (f) 600 °C taken by AFM using tapping mode. The scan area is $5 \times 5\ \mu m^2$.

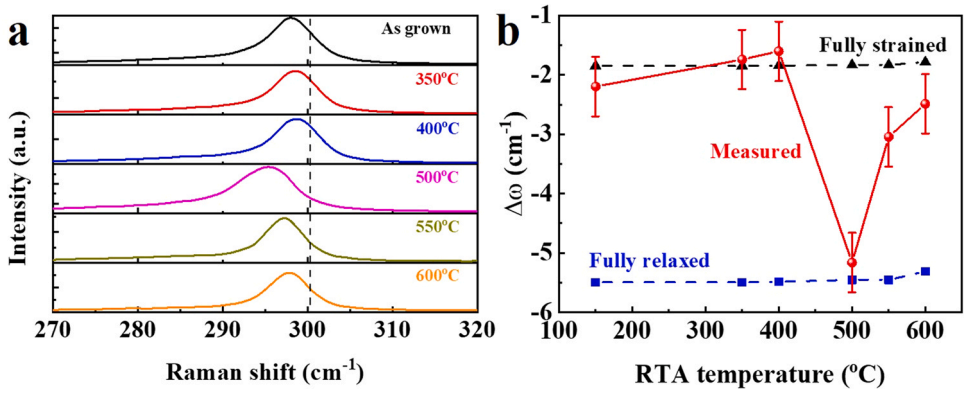

Fig. 4. (a) Raman spectra showing intensity versus wavenumber of as-grown sample and samples after RTA at 350–600 °C; (b) Dependence of Raman spectral shift for Ge-Ge mode of GeSn film on the RTA temperature.

of the Raman system is 1 cm^{-1} giving an error within ± 0.5 cm^{-1}. The peak located between 290 and 300 cm^{-1} in each plot involves both of Ge-Sn and Ge-Ge modes from GeSn. Through Lorentz fitting, the peak position of Ge-Ge mode can be extracted. The peak position of Ge-Ge mode from bulk Ge has been indicated as the vertical dash line in Fig. 4(a). The red solid line in Fig. 4(b) shows the extracted shift of Ge-Ge peak position of GeSn relative to that of bulk Ge as a function of RTA temperature. According to previous reports, the Raman spectral shift ($\Delta\omega$) is related to the in-plane strain ($\varepsilon_{//}$) and the Sn content (x) [47]:

$$\Delta\omega = ax + b\varepsilon_{//}, \tag{8}$$

where $a = -83\ cm^{-1}$ is the Raman-Sn content coefficient and $b = -375\ cm^{-1}$ is the Raman-strain shift coefficient. The incorporation of Sn and tensile strain in GeSn would lead to a negative Raman spectral shift, and a positive shift for compressive strain. The black dash line with triangular data points and blue dash line with square data points represent the calculated $\Delta\omega$ of fully strained GeSn and fully relaxed GeSn using the Sn content in Table 1 by Eq. (8), respectively. As can be seen, the $\Delta\omega$ of as-grown sample and sample annealed at 350 °C approximates the fully strained value, agreeing well with XRD measurement results. For GeSn film annealed at 400 °C, $\Delta\omega$ is still located near the fully strained value, although a strain relaxation is detected by XRD-RSM. The result indicates that the strain relaxation mainly occurs in the region near the GeSn/Ge interface. For the sample annealed at 500 °C, the measured $\Delta\omega$ is close to the fully relaxed value. However, based on the Sn content and in-plane strain from XRD-RSM results, $\Delta\omega$ should be much less negative. According to Eq. (8), the negative shift of $\Delta\omega$ can be attributed to enriched Sn content. The Sn content is observed to be higher in the surface region and this may result from Sn outdiffusion during RTA at 500 °C. As RTA temperature further rises to 550 and 600 °C, $\Delta\omega$ gradually becomes less negative mainly due to Sn segregation on surface although the strain relaxation increases.

To characterize the crystal quality of the GeSn films after thermal treatment, TEM images are taken from the samples after RTA at 350 and 500 °C. Fig. 5(a) displays the cross-sectional TEM image of the sample after RTA at 350 °C. A smooth and sharp interface between GeSn and Ge can be observed. The thickness of GeSn is verified to be ~200 nm. Fig. 5(b) shows the HRTEM image of the GeSn/Ge interface. The interface is free of misfit dislocations again confirming that GeSn is coherently grown on Ge. The inset shows the selected area electron diffraction (SAED) pattern taken from the red circular region in Fig. 5(a). The well-ordered diffraction pattern indicates a tetragonal symmetry. Fig. 5(c) zooms in on the SAED pattern of Fig. 5(b) near the (224) diffraction spot. Two sets of diffraction patterns from GeSn and Ge can be recognized. The GeSn diffraction spots lie vertically below the Ge diffraction spots due to equal in-plane lattice constant. The cross-sectional TEM and HRTEM images of the sample after RTA at 500 °C are displayed in Fig. 5(d) and 5(e), respectively. Clear misfit dislocations at the GeSn/Ge interface and dislocation loops adjacent to the GeSn/Ge interface are observed. It should be noticed that the dislocations are confined within the ~50 nm region adjacent to the GeSn/Ge interface. No Sn precipitate or Sn segregation is detected over the cross section. Fig. 5(f) shows the zoomed-in SAED pattern of the inset in Fig. 5(e) taken from the red circular region in Fig. 5(d) near the $(\bar{2}\bar{2}4)$ diffraction spot. For asymmetric lattice planes, the GeSn diffraction spots locates between the fully strained line (vertical direction) and the fully relaxed line (red dash line). The results affirm that the strain in GeSn film is partially relaxed without Sn segregation after RTA at 500 °C.

From Raman spectra, it is recalled that the sample annealed at 500 °C has highest Sn content in the surface region among all samples. To further explore the elemental distribution of the GeSn film, Ge and Sn depth profiles are taken by EDS line scans for the samples annealed at 350 and 500 °C, as shown in Fig. 6. For the sample annealed at 350 °C, Ge and Sn are distributed uniformly in the film with a Sn content of ~6.6% agreeing well with the XRD-RSM result. After RTA at 500 °C, Sn diffuses away from the GeSn/Ge interface toward sample surface and Ge substrate. The Sn content increases linearly from ~6% at depth of 175 nm to ~10% on sample surface. The results indicate that interdiffusion of Sn and Ge atoms occurs along with generation of misfit dislocations during RTA at 500 °C. The interdiffusion of Sn and Ge atoms is driven by the metastability of the GeSn film under thermal treatment. From XRD RSM and cross-section TEM images, no Sn segregation or precipitation is detected. It is inferred that Sn atoms alloy with Ge atoms in the surface region, which is probably promoted by the strain relaxation. The strain-relaxation-enhanced incorporation of Sn in GeS has been reported in CVD growth GeSn [48].

To further study the influence of thermal treatment on the optical property of the GeSn film, PL measurements were carried out. The spontaneous emission was excited by a 1064 ± 2 nm continuous laser with a spot size of ~120 μm and was collected by an InGaAs photodetector. Lock-in technique was employed to improve the signal to noise ratio at a reference frequency of 320 Hz. Fig. 7(a) compares the PL spectra of the as-grown sample and samples annealed at 200–600 °C under an excitation power of 530 mW (corresponding to a power density of ~4.69 kW/cm^2). The samples exhibit broad emission spectra between 1400 and 2400 nm with several peaks. The peak around 1600 nm is emitted from Ge direct bandgap [49], which comes from Ge region near GeSn/Ge interface. The emitted wavelength of Ge direct bandgap is a bit longer than expected probably due to existence of tensile strain induced by lattice mismatch between GeSn and Ge. After RTA at 400–600 °C, the

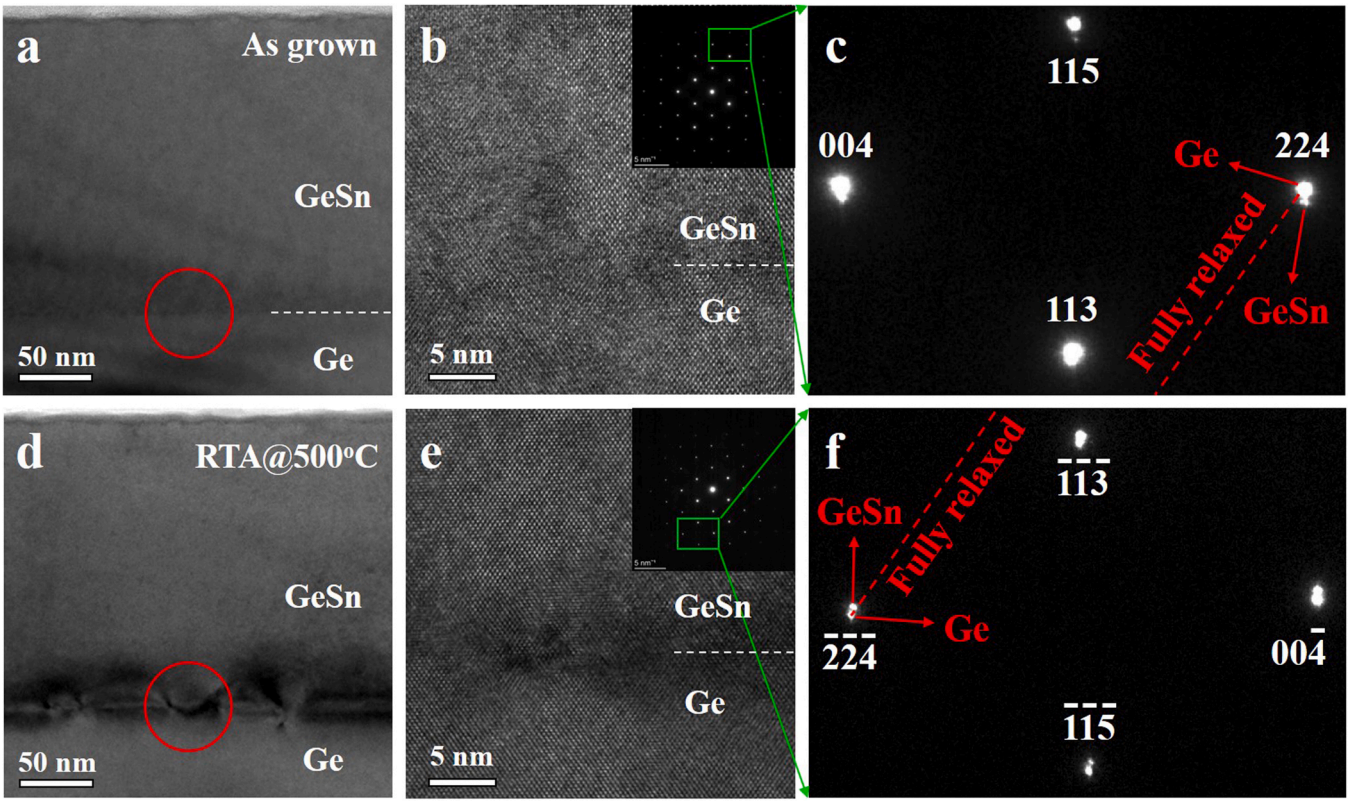

Fig. 5. (a) Cross-sectional TEM image of GeSn sample after RTA at 350 °C. (b) HRTEM image taken from the GeSn/Ge interface of the as-grown sample. The inset shows the SAED from the red circular area in Fig. 5(a). (c) Enlarged image of the SAED pattern in Fig. 5(b) around the (224) diffraction spot. (d) Cross-sectional TEM image of GeSn sample after RTA at 500 °C. (e) HRTEM image taken from the GeSn/Ge interface of the sample annealed at 500 °C. The inset shows the SAED from the red circular area in Fig. 5(d). (f) Zoomed-in image of the SAED pattern in Fig. 5(e) around the $(\bar{2}\bar{2}4)$ diffraction spot.

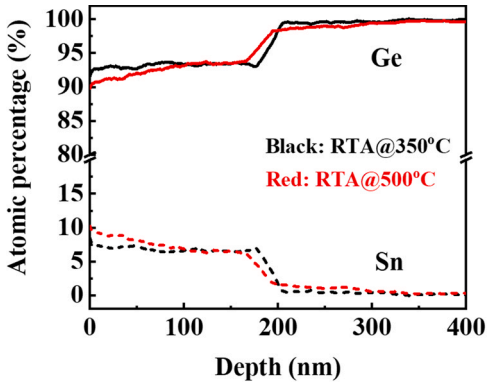

Fig. 6. Ge and Sn depth profiles showing the atomic percentages of Ge and Sn, taken from EDS line scan of GeSn sample after RTA at 500 °C.

peak position of Ge shifts to longer wavelength, which can be ascribed to diffusion of Sn into the Ge substrate after RTA at high temperature as confirmed in Fig. 6. As RTA temperature increases, the PL intensity and peak position in the range of 1800–2400 nm change appreciably. To quantitatively analyze the PL spectra, Gaussian fitting was carried out for each PL spectrum. Fig. 7(b) and 7(c) show the fitting results of PL spectra from as-grown sample and sample after RTA at 500 °C, respectively. The PL spectrum of as-grown sample can be decomposed into four peaks [50]: P1@1588 nm, P2@1934 nm, P3@2125 nm and P4@2164 nm from direct bandgap of Ge, direct bandgap of GeSn, 2nd order diffraction of pumped laser by the blaze grating and indirect bandgap of GeSn, respectively. To facilitate analysis of the optical property of GeSn, the indirect bandgap emission of Ge at around 1800 nm, which is weaker than the direct bandgap emission in tensile-strained Ge [51], is neglected. After annealing at 500 °C, P1 and P2 shifts to 1638 nm and 2088 nm, respectively. Due to detector cutoff at around 2300 nm, P4 can be only partially detected for sample annealed at 500 °C.

The black curve in Fig. 7(d) summarizes the dependence of PL peak energy from direct bandgap of GeSn (P2) on RTA temperatures. After RTA at 200 and 350 °C, the PL peak positions keep at around 0.640 eV, similar to that of as-grown sample, since the GeSn film is still fully strained after RTA at 200 and 350 °C. As RTA temperature increases to 400 and 500 °C, the P2 PL peak energy shifts to 0.615 and 0.594 eV, respectively, probably due to strain relaxation of GeSn and increased Sn content in surface region of GeSn. Both strain relaxation and enriched Sn content in GeSn decrease the bandgap of GeSn. After RTA at 550 and 600 °C, the competitive effects of Sn segregation and strain relaxation, which lead to increase and decrease of GeSn bandgap [20], respectively, result in P2 peak energies of 0.600 and 0.595 eV, respectively. The red curve in Fig. 7(d) displays the P2 PL integrated intensity of the GeSn samples as a function of RTA temperature. After RTA at 200 and 350 °C, the PL intensity slightly increases compared to that of as-grown sample due to slight improvement of crystal quality. After RTA at 400, 500, 550 and 600 °C, the PL intensity is enhanced by ~ 2.1, ~ 7.8, ~ 4.8 and ~ 2.9 fold compared to that of as-grown sample, respectively, although misfit dislocations and threading dislocations are generated. The

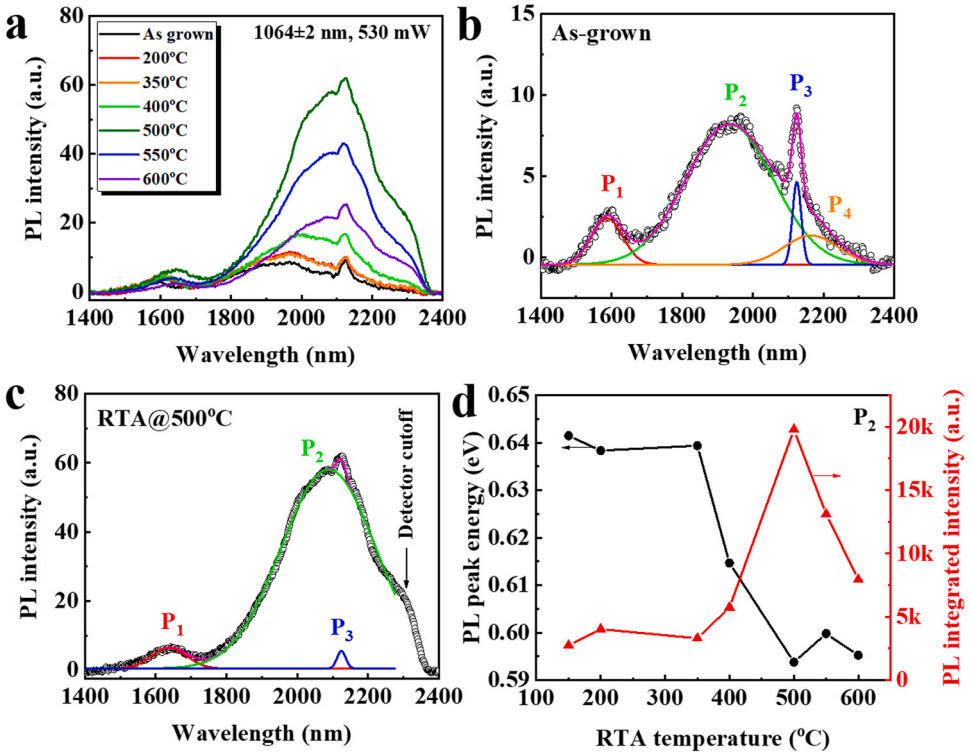

Fig. 7. (a) RT PL spectra showing PL intensity versus wavelength of as-grown sample and sample annealed at 200–600 °C. Decomposition of the PL spectra for (b) as-grown sample and (c) sample annealed at 500 °C using Gaussian fitting. P1, P2, P3 and P4 are from direct bandgap of Ge, direct bandgap of GeSn, 2nd order diffraction of pumped laser and indirect bandgap of GeSn, respectively. (d) Peak energy (black curve) and integrated intensity (red curve) of direct bandgap luminescence of GeSn as a function of RTA temperature.

enhanced PL intensity may be due to improvement of material quality and strain relaxation in GeSn. It has been reported the substitution of implanted dopants in Ge or Sn lattices can be done at 400 °C [52]. Hence, the high temperature process may repair the abundant point defects produced during low-temperature MBE of GeSn, which reduces the nonradiative recombination process. The relaxation of compressive strain enhances the GeSn direct bandgap emission relative to the indirect emission [20], which leads to higher occupation probability of electrons in Γ valley.

It is noticed that the GeSn sample has a maximum PL intensity after RTA at 500 °C. To further explore the light emitting property of the sample, power-dependent PL spectra were collected. Fig. 8(a) and 8(b) show the PL spectra of as-grown sample and the sample after RTA at 500 °C under pumping power of 172–530 mW (power density of 1.52–4.69 kW/cm^2), respectively. As pumping power increases, the PL intensities from both Ge and GeSn increases. However, the Ge emission peak shows a red shift with increased pumping power due to Joule heating effect [53] by the pumping laser. The increase of sample temperature leads to reduction of Ge direct bandgap thus the red shift of PL peak. However, the PL peak position of GeSn direct bandgap appears to be less sensitive to the pumping power. One possibility could be a competition between band filling effect and Joule heating effect under large injection, since most of photogenerated carriers are injected into GeSn and the energy difference between Γ and L valleys of GeSn is smaller than that of Ge. The black and blue curves in Fig. 8(c) depict the variation of integrated PL intensity of GeSn direct bandgap versus the pumping power for as-grown sample and the sample after RTA at 500 °C, respectively. As pumping power increases, the integrated PL intensity from both samples increases superlinearly. The red curve in Fig. 8(c) shows the ratio of the integrated PL intensity from GeSn direct bandgap between sample after RTA at 500 °C and the as-grown sample as a function of the pumping power. Under pumping power of 172, 270, 390 and 530 mW, the intensity ratio is around 22.8, 11.2, 8.7 and 7.8, respectively. The results indicate that the sample annealed at 500 °C has much higher light emitting efficiency than that of as-grown sample, especially under low injection conditions. The results indicate that RTA can be an effective approach to enhance the light emitting property of GeSn.

The dramatically enhanced light emitting efficiency of GeSn sample after RTA at 500 °C may be mainly attributed to the following two contributions. First, the thermal treatment at 500 °C may repair the point defects in GeSn and enables the relaxation of compressive strain, which suppresses the nonradiative combination process and reduces the energy difference between Γ and L valleys, respectively, as mentioned above. Another possible factor contributing to the enhanced PL intensity of GeSn annealed at 500 °C is formation of Sn gradient. As analyzed in Fig. 6, the Sn content gradually increases from ~6% at depth of 175 nm to ~10% on sample surface, which naturally forms a Sn-component-gradual (SCG) heterojunction in GeSn, as shown in Fig. 8(d). The SCG heterojunction has lower energy for electrons in Γ valley and holes in heavy hole (HH) valence band [54] in the surface region rendering spontaneous transportation of optically pumped carriers from GeSn/Ge interface to the surface region. The carriers are confined at the surface region with high crystal quality reducing the nonradiative recombination process at the defective region near the GeSn/Ge interface. Meanwhile, the GeSn film has higher light emitting efficiency in the surface region due to higher Sn content, since the energy difference between Γ and L valleys reduces with increasing Sn content resulting in higher occupation probability of electrons in the Γ valley. Additionally, the spontaneous emission near the surface region also reduces the self-absorption [49] process in GeSn thus increasing the light extraction efficiency from GeSn.

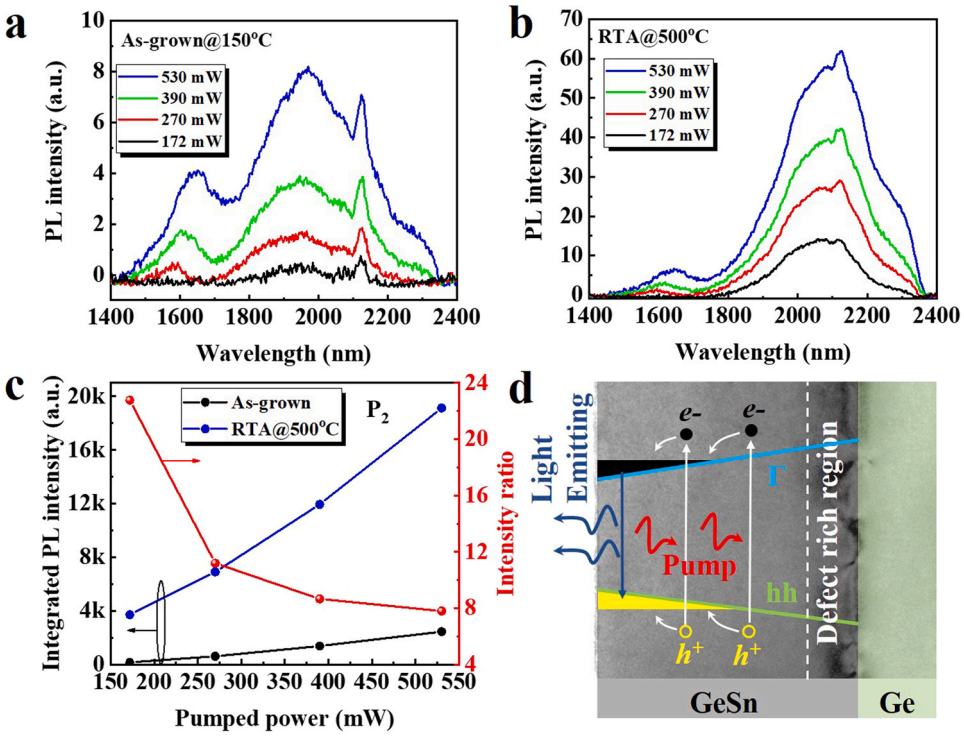

Fig. 8. RT PL spectra of (a) as-grown sample and (b) sample annealed at 500 °C under pumping power of 172–530 mW. (c) Dependence of integrated PL intensity (red curve) of GeSn direct band on pumping power for as-grown sample (black line) and sample annealed at 500 °C (blue line). The ratio of integrated PL intensity of GeSn direct band between as-grown sample and sample annealed at 500 °C as a function of pumping power is also plotted (red line). (d) Schematic diagram of the band alignment for Γ conduction band and heavy hole (hh) valence band in the GeSn film. The photogenerated carriers are spontaneously confined in the surface region due to higher Sn content, which has high crystal quality with relaxed strain.

4. Conclusion

In summary, the influence of rapid thermal annealing (RTA) on the structural and optical properties of 200 nm pseudomorphic GeSn film on Ge (001) substrate grown by low-temperature molecular beam epitaxy (MBE) has been investigated. The GeSn film maintains fully strained state after RTA at temperatures up to 350 °C. Under RTA at 400–500 °C, the strain relaxation of GeSn film is enabled due to generation of misfit dislocations and increases with increasing temperature. Outdiffusion of Sn is observed in GeSn after RTA at 500 °C. At annealing temperatures of 550 °C or higher, Sn segregation occurs along with the strain relaxation. The PL intensity of the annealed samples is enhanced compared to that of as-grown sample probably due to improved crystal quality and strain relaxation (for annealing at temperatures above 350 °C) of GeSn. It is found that the GeSn sample annealed at 500 °C has a maximum PL intensity, which may be attributed to formation of a SCG heterojunction with highest Sn content in surface region. The photogenerated carriers are confined in the surface region resulting in dramatically enhanced light emitting efficiency, which can be ascribed to enlarged occupation probability of carriers in Γ valley, reduced self-absorption of GeSn in the surface region and reduced nonradiative recombination processes near the GeSn/Ge interface. The results indicate that RTA can be a simple but effective approach to improve the light emitting property of GeSn grown by low-temperature MBE.

CRediT authorship contribution statement

Guangyang Lin: Conceptualization, Investigation, Writing – original draft, Funding acquisition. **Kun Qian:** Investigation, Data curation, Validation. **Hongjie Cai:** Methodology, Visualization. **Haochen Zhao:** Methodology. **Jianfang Xu:** Methodology. **Songyan Chen:** Formal analysis. **Cheng Li:** Supervision, Writing – review & editing. **Ryan Hickey:** Methodology. **James Kolodzey:** Formal analysis. **Yuping Zeng:** Supervision, Writing – review & editing.

Declaration of Competing Interest

The authors declare that they have no known competing financial interests or personal relationships that could have appeared to influence the work reported in this paper.

Acknowledgment

This work was supported by National Natural Science Foundation of China under Grant no. 62104205, the Fundamental Research Funds for the Central Universities under Grant no. 20720210019. We greatly appreciate Dr. Xiangquan Liu and Prof. Jun Zheng from Institute of Semiconductors of Chinese Academy of Sciences for their help in XRD-RSM measurements. This work is also supported in part by the NASA International Space Station (NASA ISS) under Grant 80NSSC20M0142, and in part by Air Force Office of Scientific Research under Grants FA9550-19-1-0297 and FA9550-21-1-0076.

References

[1] A. Gassenq, F. Gencarelli, J. Van Campenhout, Y. Shimura, R. Loo, G. Narcy, B. Vincent, G. Roelkens, GeSn/Ge heterostructure short-wave infrared photodetectors on silicon, Opt. Express 20 (2012) 27297–27303.
[2] H. Tran, T. Pham, J. Margetis, Y. Zhou, W. Dou, P.C. Grant, J.M. Grant, S. Al-Kabi, G. Sun, R.A. Soref, J. Tolle, Y.-H. Zhang, W. Du, B. Li, M. Mortazavi, S.-Q. Yu, Si-Based GeSn photodetectors toward mid-infrared imaging applications, ACS Photonics 6 (2019) 2807–2815.
[3] S. Wirths, R. Geiger, N. von den Driesch, G. Mussler, T. Stoica, S. Mantl, Z. Ikonic, M. Luysberg, S. Chiussi, J.M. Hartmann, H. Sigg, J. Faist, D. Buca, D. Grützmacher, Lasing in direct-bandgap GeSn alloy grown on Si, Nat. Photonics 9 (2015) 88–92.

[4] A. Gassenq, L. Milord, J. Aubin, K. Guilloy, S. Tardif, N. Pauc, J. Rothman, A. Chelnokov, J.M. Hartmann, V. Reboud, V. Calvo, Gamma bandgap determination in pseudomorphic GeSn layers grown on Ge with up to 15% Sn content, Appl. Phys. Lett. 109 (2016) 242107.

[5] W. Du, S.A. Ghetmiri, B.R. Conley, A. Mosleh, A. Nazzal, R.A. Soref, G. Sun, J. Tolle, J. Margetis, H.A. Naseem, S.-Q. Yu, Competition of optical transitions between direct and indirect bandgaps in Ge1−xSnx, Appl. Phys. Lett. 105 (2014) 051104.

[6] H. Tran, W. Du, S.A. Ghetmiri, A. Mosleh, G. Sun, R.A. Soref, J. Margetis, J. Tolle, B. Li, H.A. Naseem, S.-Q. Yu, Systematic study of Ge1−xSnx absorption coefficient and refractive index for the device applications of Si-based optoelectronics, J. Appl. Phys. 119 (2016) 103106.

[7] N. von den Driesch, D. Stange, S. Wirths, G. Mussler, B. Holländer, Z. Ikonic, J.M. Hartmann, T. Stoica, S. Mantl, D. Grützmacher, D. Buca, Direct bandgap group IV epitaxy on Si for laser applications, Chem. Mater. 27 (2015) 4693–4702.

[8] H.H. Tseng, K.Y. Wu, H. Li, V. Mashanov, H.H. Cheng, G. Sun, R.A. Soref, Mid-infrared electroluminescence from a Ge/Ge0.922Sn0.078/Ge double heterostructure p-i-n diode on a Si substrate, Appl. Phys. Lett. 102 (2013) 182106.

[9] D. Stange, N. von den Driesch, D. Rainko, S. Roesgaard, I. Povstugar, J.-M. Hartmann, T. Stoica, Z. Ikonic, S. Mantl, D. Grützmacher, D. Buca, Short-wave infrared LEDs from GeSn/SiGeSn multiple quantum wells, Optica 4 (2017) 185–188.

[10] L. Peng, X. Li, J. Zheng, X. Liu, M. Li, Z. Liu, C. Xue, Y. Zuo, B. Cheng, Room-temperature direct-bandgap electroluminescence from type-I GeSn/SiGeSn multiple quantum wells for 2 μm LEDs, J. Lumin. 228 (2020) 117539.

[11] J.D. Gallagher, C.L. Senaratne, P. Sims, T. Aoki, J. Menéndez, J. Kouvetakis, Electroluminescence from GeSn heterostructure pin diodes at the indirect to direct transition, Appl. Phys. Lett. 106 (2015) 091103.

[12] V. Reboud, A. Gassenq, N. Pauc, J. Aubin, L. Milord, Q.M. Thai, M. Bertrand, K. Guilloy, D. Rouchon, J. Rothman, T. Zabel, F. Armand Pilon, H. Sigg, A. Chelnokov, J.M. Hartmann, V. Calvo, Optically pumped GeSn micro-disks with 16% Sn lasing at 3.1 μm up to 180 K, Appl. Phys. Lett. 111 (2017) 092101.

[13] A. Elbaz, D. Buca, N. von den Driesch, K. Pantzas, G. Patriarche, N. Zerounian, E. Herth, X. Checoury, S. Sauvage, I. Sagnes, A. Foti, R. Ossikovski, J.-M. Hartmann, F. Boeuf, Z. Ikonic, P. Boucaud, D. Grützmacher, M. El Kurdi, Ultra-low-threshold continuous-wave and pulsed lasing in tensile-strained GeSn alloys, Nat. Photonics 14 (2020) 375–382.

[14] B. Wang, E. Sakat, E. Herth, M. Gromovyi, A. Bjelajac, J. Chaste, G. Patriarche, P. Boucaud, F. Boeuf, N. Pauc, V. Calvo, J. Chrétien, M. Frauenrath, A. Chelnokov, V. Reboud, J.-M. Hartmann, M. El Kurdi, GeSnOI mid-infrared laser technology, Light: Sci. Appl. 10 (2021) 232.

[15] H.-J. Joo, Y. Kim, D. Burt, Y. Jung, L. Zhang, M. Chen, S.J. Parluhutan, D.-H. Kang, C. Lee, S. Assali, Z. Ikonic, O. Moutanabbir, Y.-H. Cho, C.S. Tan, D. Nam, 1D photonic crystal direct bandgap GeSn-on-insulator laser, Appl. Phys. Lett. 119 (2021) 201101.

[16] Y. Zhou, Y. Miao, S. Ojo, H. Tran, G. Abernathy, J.M. Grant, S. Amoah, G. Salamo, W. Du, J. Liu, J. Margetis, J. Tolle, Y.-h. Zhang, G. Sun, R.A. Soref, B. Li, S.-Q. Yu, Electrically injected GeSn lasers on Si operating up to 100 K, Optica 7 (2020) 924–928.

[17] Y. Zhou, S. Ojo, C.-W. Wu, Y. Miao, H. Tran, J.M. Grant, G. Abernathy, S. Amoah, J. Bass, G. Salamo, W. Du, G.-E. Chang, J. Liu, J. Margetis, J. Tolle, Y.-H. Zhang, G. Sun, R.A. Soref, B. Li, S.-Q. Yu, Electrically injected GeSn lasers with peak wavelength up to 2.7 μm, Photonics Res. 10 (2022) 222–229.

[18] R.W. Olesinski, G.J. Abbaschian, The Ge–Sn (Germanium–Tin) system, Bull. Alloy Phase Diagr. 5 (1984) 265–271.

[19] S. Wirths, D. Buca, S. Mantl, Si–Ge–Sn alloys: from growth to applications, Prog. Cryst. Growth Charact. Mater. 62 (2016) 1–39.

[20] S. Gupta, B. Magyari-Köpe, Y. Nishi, K.C. Saraswat, Achieving direct band gap in germanium through integration of Sn alloying and external strain, J. Appl. Phys. 113 (2013) 073707.

[21] N. Bhargava, M. Coppinger, J. Prakash Gupta, L. Wielunski, J. Kolodzey, Lattice constant and substitutional composition of GeSn alloys grown by molecular beam epitaxy, Appl. Phys. Lett. 103 (2013) 041908.

[22] R. Hickey, N. Fernando, S. Zollner, J. Hart, R. Hazbun, J. Kolodzey, Properties of pseudomorphic and relaxed germanium1−xtinx alloys (x < 0.185) grown by MBE, J. Vac. Sci. Technol. B 35 (2017) 021205.

[23] M. Oehme, K. Kostecki, M. Schmid, F. Oliveira, E. Kasper, J. Schulze, Epitaxial growth of strained and unstrained GeSn alloys up to 25% Sn, Thin Solid Films 557 (2014) 169–172.

[24] L. Wei, Y. Miao, R. Pan, W.-w. Zhang, C. Li, H. Lu, Y.-F. Chen, Highly strained Ge1-xSnx alloy films with high Sn compositions grown by MBE, J. Cryst. Growth 557 (2021) 125996.

[25] H.-J. Jo, M.G. So, J.S. Kim, M.-Y. Ryu, Y.K. Yeo, J. Kouvetakis, Temperature-dependent direct transition energy in Ge0.99Sn0.01 film grown on Si measured by photoreflectance spectroscopy, Thin Solid Films 591 (2015) 295–300.

[26] J. Aubin, J.M. Hartmann, GeSn growth kinetics in reduced pressure chemical vapor deposition from Ge2H6 and SnCl4, J. Cryst. Growth 482 (2018) 30–35.

[27] B. Vincent, F. Gencarelli, H. Bender, C. Merckling, B. Douhard, D.H. Petersen, O. Hansen, H.H. Henrichsen, J. Meersschaut, W. Vandervorst, M. Heyns, R. Loo, M. Caymax, Undoped and in-situ B doped GeSn epitaxial growth on Ge by atmospheric pressure-chemical vapor deposition, Appl. Phys. Lett. 99 (2011) 152103.

[28] A.C. Meng, M.R. Braun, Y. Wang, S. Peng, W. Tan, J.Z. Lentz, M. Xue, A. Pakzad, A.F. Marshall, J.S. Harris, W. Cai, P.C. McIntyre, Growth mode control for direct-gap core/shell Ge/GeSn nanowire light emission, Mater. Today 40 (2020) 101–113.

[29] X. Liu, J. Zheng, M. Li, F. Wan, C. Niu, Z. Liu, Y. Zuo, C. Xue, B. Cheng, Growth of relaxed GeSn film with high Sn content via Sn component-grade buffer layer structure, J. Phys. D: Appl. Phys. 54 (2021) 435101.

[30] J. Zheng, S. Wang, Z. Liu, H. Cong, C. Xue, C. Li, Y. Zuo, B. Cheng, Q. Wang, GeSn p-i-n photodetectors with GeSn layer grown by magnetron sputtering epitaxy, Appl. Phys. Lett. 108 (2016) 033503.

[31] H. Groiss, M. Glaser, M. Schatzl, M. Brehm, D. Gerthsen, D. Roth, P. Bauer, F. Schäffler, Free-running Sn precipitates: an efficient phase separation mechanism for metastable Ge1−xSnx epilayers, Sci. Rep. 7 (2017) 16114.

[32] G. Han, Y. Wang, Y. Liu, C. Zhang, Q. Feng, M. Liu, S. Zhao, B. Cheng, J. Zhang, Y. Hao, GeSn quantum well P-channel tunneling FETs fabricated on Si(001) and (111) with improved subthreshold swing, IEEE Electron Device Lett. 37 (2016) 701–704.

[33] M. Oehme, M. Schmid, M. Kaschel, M. Gollhofer, D. Widmann, E. Kasper, J. Schulze, GeSn p-i-n detectors integrated on Si with up to 4% Sn, Appl. Phys. Lett. 101 (2012) 141110.

[34] Y.-H. Huang, G.-E. Chang, H. Li, H.H. Cheng, Sn-based waveguide p-i-n photodetector with strained GeSn/Ge multiple-quantum-well active layer, Opt. Lett. 42 (2017) 1652–1655.

[35] J. Rathore, A. Nanwani, S. Mukherjee, S. Das, O. Moutanabbir, S. Mahapatra, Composition uniformity and large degree of strain relaxation in MBE-grown thick GeSn epitaxial layers, containing 16% Sn, J. Phys. D: Appl. Phys. 54 (2021) 185105.

[36] K.A. Bratland, Y.L. Foo, T. Spila, H.S. Seo, R.T. Haasch, P. Desjardins, J.E. Greene, Sn-mediated Ge⁄Ge(001) growth by low-temperature molecular-beam epitaxy: surface smoothening and enhanced epitaxial thickness, J. Appl. Phys. 97 (2005) 044904.

[37] H. Li, Y.X. Cui, K.Y. Wu, W.K. Tseng, H.H. Cheng, H. Chen, Strain relaxation and Sn segregation in GeSn epilayers under thermal treatment, Appl. Phys. Lett. 102 (2013) 251907.

[38] W. Wang, L. Li, Q. Zhou, J. Pan, Z. Zhang, E.S. Tok, Y.-C. Yeo, Tin surface segregation, desorption, and island formation during post-growth annealing of strained epitaxial Ge1−xSnx layer on Ge(001) substrate, Appl. Surf. Sci. 321 (2014) 240–244.

[39] P. Zaumseil, Y. Hou, M.A. Schubert, N. von den Driesch, D. Stange, D. Rainko, M. Virgilio, D. Buca, G. Capellini, The thermal stability of epitaxial GeSn layers, APL Mater. 6 (2018) 076108.

[40] N. von den Driesch, S. Wirths, R. Troitsch, G. Mussler, U. Breuer, O. Moutanabbir, D. Grützmacher, D. Buca, Thermally activated diffusion and lattice relaxation in (Si)GeSn materials, Phys. Rev. Mater. 4 (2020) 033604.

[41] R. Chen, Y.-C. Huang, S. Gupta, A.C. Lin, E. Sanchez, Y. Kim, K.C. Saraswat, T.I. Kamins, J.S. Harris, Material characterization of high Sn-content, compressively-strained GeSn epitaxial films after rapid thermal processing, J. Cryst. Growth 365 (2013) 29–34.

[42] L. Wang, Y. Zhang, Y. Wu, T. Liu, Y. Miao, L. Meng, Z. Jiang, H. Hu, Effects of annealing on the behavior of Sn in GeSn alloy and GeSn-based photodetectors, IEEE Trans. Electron Devices 67 (2020) 3229–3234.

[43] O. Olorunsola, H. Stanchu, S. Ojo, K. Pandey, A. Said, J. Margetis, J. Tolle, A. Kuchuk, Y.I. Mazur, G. Salamo, S.-Q. Yu, Impact of long-term annealing on photoluminescence from Ge1−xSnx alloys, Crystals 11 (2021).

[44] J.S. Hovis, R.J. Hamers, C.M. Greenlief, Preparation of clean and atomically flat germanium(001) surfaces, Surf. Sci. 440 (1999) L815–L819.

[45] W.X. Ni, K. Lyutovich, J. Alami, C. Tengstedt, M. Bauer, E. Kasper, X-ray reciprocal space mapping studies of strain relaxation in thin SiGe layers (⩽100nm) using a low temperature growth step, J. Cryst. Growth 227–228 (2001) 756–760.

[46] G. Lin, D. Liang, J. Wang, C. Yu, C. Li, S. Chen, W. Huang, J. Wang, J. Xu, Strain evolution in SiGe-on-insulator fabricated by a modified germanium condensation technique with gradually reduced condensation temperature, Mater. Sci. Semicond. Process. 97 (2019) 56–61.

[47] R. Cheng, W. Wang, X. Gong, L. Sun, P. Guo, H. Hu, Z. Shen, G. Han, Y.-C. Yeo, Relaxed and strained patterned germanium-tin structures: a Raman scattering study, ECS J. Solid State Sci. Technol. 2 (2013) P138–P145.

[48] S. Assali, J. Nicolas, O. Moutanabbir, Enhanced Sn incorporation in GeSn epitaxial semiconductors via strain relaxation, J. Appl. Phys. 125 (2019) 025304.

[49] G. Lin, X. Yi, C. Li, N. Chen, L. Zhang, S. Chen, W. Huang, J. Wang, X. Xiong, J. Sun, Strong room temperature electroluminescence from lateral p-SiGe/i-Ge/n-SiGe heterojunction diodes on silicon-on-insulator substrate, Appl. Phys. Lett. 109 (2016) 141104.

[50] S.A. Ghetmiri, W. Du, J. Margetis, A. Mosleh, L. Cousar, B.R. Conley, L. Domulevicz, A. Nazzal, G. Sun, R.A. Soref, J. Tolle, B. Li, H.A. Naseem, S.-Q. Yu, Direct-bandgap GeSn grown on silicon with 2230 nm photoluminescence, Appl. Phys. Lett. 105 (2014) 151109.

[51] D. Nam, D. Sukhdeo, S.-L. Cheng, A. Roy, K. Chih-Yao Huang, M. Brongersma, Y. Nishi, K. Saraswat, Electroluminescence from strained germanium membranes and implications for an efficient Si-compatible laser, Appl. Phys. Lett. 100 (2012) 131112.

[52] L. Wang, S. Su, W. Wang, Y. Yang, Y. Tong, B. Liu, P. Guo, X. Gong, G. Zhang, C. Xue, B. Cheng, G. Han, Y.C. Yeo, Germanium–tin {n}{+}{/p} junction formed using phosphorus ion implant and 400 (°) {C} rapid thermal anneal, IEEE Electron Device Lett., vol. 33, 2012, pp. 1529–31.

[53] G. Lin, N. Chen, L. Zhang, Z. Huang, W. Huang, J. Wang, J. Xu, S. Chen, C. Li, Room temperature electroluminescence from tensile-strained Si0.13Ge0.87/Ge multiple quantum wells on a Ge virtual substrate, Materials 9 (2016) 803.

[54] N.S. Fernando, R.A. Carrasco, R. Hickey, J. Hart, R. Hazbun, S. Schoeche, J.N. Hilfiker, J. Kolodzey, S. Zollner, Band gap and strain engineering of pseudomorphic Ge1−x−ySixSny alloys on Ge and GaAs for photonic applications, J. Vac. Sci. Technol. B 36 (2018) 021202.